This is a peer-reviewed, author's accepted manuscript of the following research article:
Zhang, J., Alfadhl, Y., Chen, X., Zhang, L., & Cross, A. W. (2022).
Design, simulation, and cold test of a W-band double nonparallel staggered grating backward wave oscillator.
IEEE Transactions on Electron Devices, 1-5. https://doi.org/10.1109/TED.2022.3195484

Design, Simulation, and Cold Test of a *W*-Band Double Nonparallel Staggered Grating Backward Wave Oscillator

Jin Zhang, *Member, IEEE*, Yasir Alfadhl, *Senior Member, IEEE*, Xiaodong Chen, *Fellow, IEEE*, Liang Zhang, *Senior Member, IEEE*, and Adrian W. Cross, *Member, IEEE*

***Abstract*— A novel double nonparallel staggered grating (DNPSG) slow wave structure (SWS) is proposed to enhance the coupling impedance in a *W*-band backward wave oscillator (BWO) driven by a pseudospark-sourced sheet electron beam. The DNPSG SWS has been shown a broadband of 72–125 GHz and a higher coupling impedance compared with the traditional double staggered grating (DSG) SWS in simulation. The DNPSG BWO structure consisting of ten SWS units and a broadband output structure is designed and fabricated. In the cold test of the DNPSG BWO, the measured S_{11} (double of the losses in the DNPSG BWO) is above −10 dB in most of the band, which is satisfactory in the pseudospark-driven high-power device. The hot-test performance of the DNPSG BWO is analyzed by particle-in-cell (PIC) simulation in a beam voltage range of 14–90 kV and a current density range of 1.5–5 × 10^7 A/m^2, obtaining a high output power (max. 190 kW) over an ultra-wide tuning band of 38 GHz (75–113 GHz) due to enhanced coupling impedance.**

***Index Terms*— Backward wave oscillator (BWO), double nonparallel staggered grating (DNPSG), millimeter (mm) wave, pseudospark, slow wave structure (SWS).**

I. Introduction

DESPITE the development of solid-state electron devices over the years, the vacuum electron devices (VEDs), such as the traveling wave tube (TWT), backward wave oscillator (BWO), extended interaction klystron oscillator (EIKO), and magnetron, still play an important role on both commercial and military platforms due to their high output power, while solid-state sources are limited by their relatively low power in millimeter (mm)-wave and terahertz (THz) frequency bands [1]. Among the VED mm-wave and THz sources, the BWO stands out owing to its intrinsic wide frequency tuning band [2], [3]. The slow wave structure (SWS), which enables the interaction between the electron beam and the electromagnetic wave, is a core part of the BWO. The traditional helix SWS in the microwave band is limited by its power capability and complicated fabrication at the high frequencies. The double staggered grating (DSG) has been used due to its high coupling impedance and good machinability [4]–[6], e.g., recently, a DSG SWS has been investigated to work in 90–100 GHz [7]. High-power BWO with greater tuning bandwidth is attractive for applications, such as fusion plasma applications [8], [9], electron spin resonance (ESR), and nuclear magnetic resonance (NMR) [10].

To further extend the tunability of the BWO, we propose a novel double nonparallel staggered grating (DNPSG) SWS on the benchmark of DSG SWS, with the advantage of enhanced coupling impedance. Using the proposed DNPSG SWS, we have designed and fabricated a *W*-band BWO driven by a psedudospark-sourced high-current sheet beam to achieve the benefits of broadband, high power, compactness, and low cost.

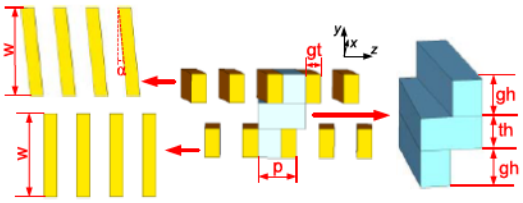

Fig. 1. Model of DNPSG SWS.

II. Design of DNPSG SWS

As shown in Fig. 1, the proposed DNPSG SWS consists of two rows of gratings opposite to each other in a staggered pattern, but it differs with the conventional DSG SWS in that the top and bottom grating rows are not parallel, i.e., the top gratings are tilted by an angle α. By optimizing the tilting angle α, it can demonstrate higher coupling impedance than the DSG SWS in the working band, thus enhancing the beam–wave interaction. The model of a DNPSG SWS unit is

Jin Zhang, Yasir Alfadhl, and Xiaodong Chen are with the School of Electronic Engineering and Computer Science, Queen Marry University of London, London E1 4NS, U.K. (e-mail: xiaodong.chen@qmul.ac.uk).
Liang Zhang and Adrian W. Cross are with the Department of Physics, University of Strathclyde, Glasgow G4 0NG, U.K. (e-mail: a.w.cross@strath.ac.uk).

TABLE I
DIMENSIONAL PARAMETERS OF DNPSG SWS

Parameters	Value	Description
w	2.052 mm	SWS width
th	0.418 mm	Height of beam tunnel
p	0.76 mm	Period
gh	0.5 mm	Height of grating
gt	0.304 mm	Thickness of grating
α	6°	Tilting angle

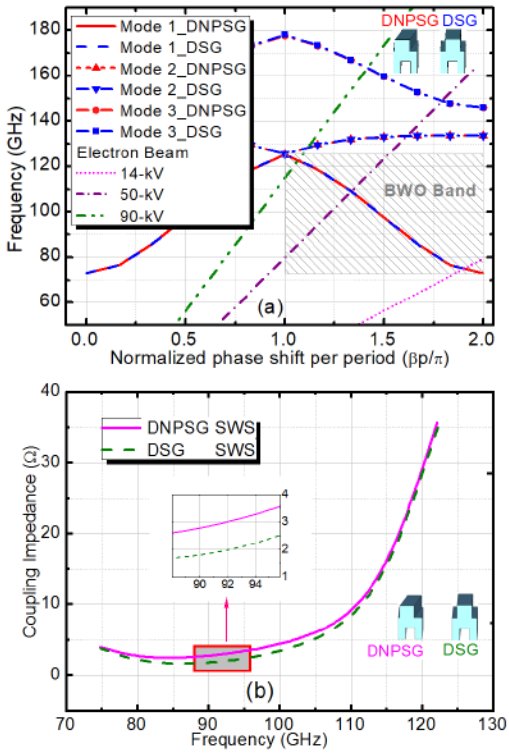

Fig. 2. Simulation results of high-frequency characteristics of novel DNPSG and conventional DSG SWSs. (a) Dispersion. (b) Coupling impedance.

built in CST Microwave Studio, in which the grating material is oxygen-free high-conductivity (OFHC) copper modeled with a conductivity of 1.17×10^7 S/m [11]. The parameters of the structure are optimized through simulation to enable operation in the entire W-band, and the optimized parameters are shown in Table I, among which the tilting angle is 6°. The tilting angle is also obtained by optimization, and its target is to find the angle where the coupling impedance is maximum while adjusting the tilting angle in the range 0°–90°.

Simulation results of the DNPSG SWS are shown in Fig. 2, in contrast with the conventional DSG SWS with the same parameters (the results of the conventional DSG SWS have been presented in a previous conference [12]). Fig. 2(a) shows the dispersion curves of modes 1–3 in the DNPSG and DSG SWSs, as well as the beamlines of 14, 50, and 90 kV. There is only a negligible difference in the dispersion curves (<1%) between the DNPSG and DSG SWSs, as the tilting angle in the DNPSG SWS (6°) is not great and only one side of the gratings is tilted. Backward wave oscillation typically occurs on the right side of the curves of mode 1 (gray shaded area), where the beamlines intersect with the mode lines, showing a wide tuning band from 72 to 125 GHz (53 GHz). The right-hand side of mode 3 in the SWSs is also backward wave, and the interaction with the electron beam could also result in backward wave oscillation and bring mode competition, which would be analyzed in detail in Section III. The gaps between modes 1 and 2 in the DNPSG and DSG SWS are 0.11 and 0.03 GHz at π point, respectively, which are relatively small, and it can be considered that the two modes (1 and 2) coalesce at π point [13], [14]. However, it is not possible to get an electron beam beyond 90 keV in our current pseudospark setup, as shown by green dashed-dotted line in Fig. 2(a), and the operation using mode 2 is not considered in this article.

The coupling impedance of mode 1 (backward wave region) in the DNPSG/DSG SWSs is also obtained through simulation in CST Microwave Studio, as shown in Fig. 2(b), and the values are calculated on the axis of the SWS. The coupling impedance of the DNPSG SWS varies between 2 and 10 Ω in W-band (75–110 GHz) and grows greater beyond 110 GHz. The comparison shows that the magnitude of the coupling impedance in the DNPSG SWS is 2.3%–55.3% greater than that in the DSG SWS, implying enhanced beam–wave interaction capability of the DNPSG SWS. The improvement in coupling impedance is significant (11.2%–55.3%) in the band 78–108 GHz, where the greatest improvement (55.3%) occurs at 89.1 GHz, as shown in the enlarged view on the top right of Fig. 2. For the rest of the tuning band, the improvement is less significant (2.3%–11.2%). The physics behind the increase of the coupling impedance is as follows. In the DSG SWS, the longitudinal electric field in the beam tunnel is mainly concentrated near the grating tops [15]; a similar distribution is also found in the DNPSG SWS. However, due to the tilting angle of the gratings in the DNPSG SWS, the grating top has greater longitudinal span, meaning that the area of electric field concentration has greater longitudinal distance, which results in longer interaction distance for the electron beam in an SWS unit. The enhanced coupling impedance has been verified by a similar work of a novel chevron-shaped DSG waveguide SWS for THz TWTs [16], but our design has the advantage of easy fabrication due to the straight-line shape of both the top tilted and bottom normal gratings, while the chevron shape would have additional fabrication challenges. So, a prototype of our design has been fabricated and will be analyzed in later chapters. Additionally, we have considered tilting on both grating rows, but the tilting of one grating row demonstrates better performance. Also, tilting on either top gratings or bottom gratings makes no difference due to the symmetry of the structure.

III. ANALYSIS ON BWO PERFORMANCE

A. Cold-Test Analysis

Using the optimized SWS, we have designed the full structure of the DNPSG BWO, as shown in Fig. 3. There are ten SWS units, followed by the output structure including a tapered DNPSG, two bent rectangular waveguides, a straight rectangular waveguide, and an expanding rectangular waveguide transitioning into the output port (port 1, WR10 port), guiding the signal out with minimal reflection in a wide

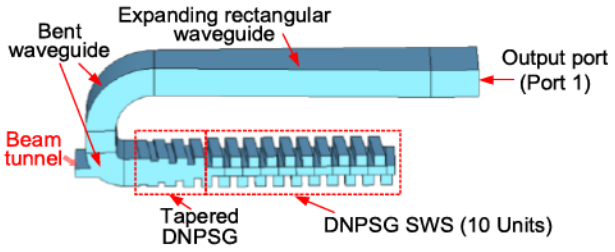

Fig. 3. Model of DNPSG BWO in CST.

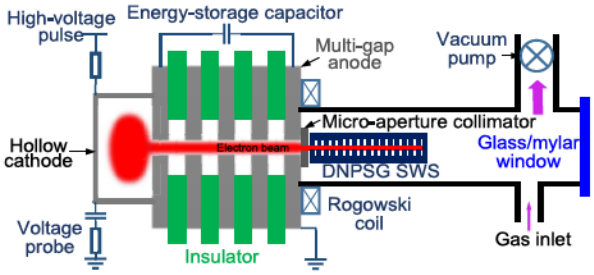

Fig. 5. Multigap pseudospark discharge setup.

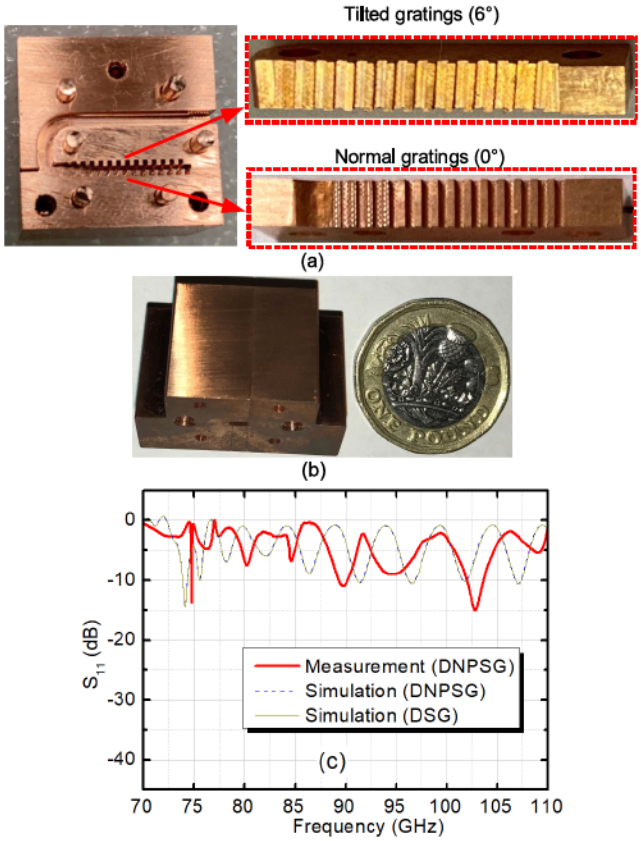

Fig. 4. Cold-test experiment of DNPSG BWO. (a) Fabricated parts of DNPSG BWO. (b) Assembled DNPSG BWO. (c) Simulated and measured S_{11} of DNPSG BWO and simulated S_{11} of DSG BWO.

frequency band. The tapered DNPSG (four units) between the normal DNPSG SWS and the bent waveguide has linearly decreasing grating heights from its right end to its left end, using the same technique as in our previous work [15]. The design is for proof-of-concept experiment and will run in burst pulsed mode, and the pseudospark electron beam also has short pulse duration; therefore, the current design without a collector works. Also, the wave will be cut off by the beam tunnel; therefore, the short end will not cause additional reflection to the circuit. The collector and output window will be considered in the upgraded version and allow the BWO to operate in the repetition mode.

The DNPSG BWO is fabricated, and its cold test has been conducted, as shown in Fig. 4. Precision computer numerical control (CNC) machining with fabrication error less than 5 μm is utilized to fabricate the BWO parts, as shown in Fig. 4(a), including the upper gratings with 6° tilting angle and the lower grating without tilting. The dimensions of the DNPSG SWS are the same with the simulation model, i.e., the same with Table I. Fig. 4(b) shows the assembled DNPSG BWO with a compact size of 28 × 16 × 17 mm^3. The DNPSG BWO is an oscillator with just one port, so only S_{11} can be measured in the cold test with a vector network analyzer (VNA). To rule out the influence of the coupler of the VNA when measuring S_{11}, measurements are conducted with and without a short-circuit metal blocker inserted between the coupler and the DNPSG BWO for bypassing, and we use the difference between the two measurements (with and without a short-circuit metal blocker) as an ideal S_{11}, i.e., excluding port mismatch, only including double of the losses of the BWO structure. The results in Fig. 4(c) show that in most of the W-band, the measured S_{11} is above -10 dB except a few points, and it agrees with simulation results, showing that the loss of the cavity of the DNPSG BWO is acceptable, considering the enormous power generated as shown in Section III-B. The resonance peaks are mainly caused by the long output waveguide, and the main difference between the simulation and measurement is the shift in the frequency, due to the same reason caused by the long output waveguide. Fig. 4(c) also shows the comparison of S_{11} between the DNPSG BWO and the DSG BWO, and the difference is negligible. This is because the tilting angle is only 6°, which is tiny.

B. Wideband Hot-Test Simulation

We use pseudospark plasma cathode as the generator of a high-current electron beam to drive the DNPSG BWO, as shown in Fig. 5. When a high-voltage pulse is applied to the hollow cathode (the cavity on the left end of Fig. 5) filled with 50–500-mtorr Argon gas, the pseudospark discharge occurs, releasing a huge number of electrons [17], [18]. We use a collimator with a rectangular aperture attached to the anode to extract the sheet beam, and an electron beam with the current density up to 10^8 A/m^2 will transmit through the anode hole, which is similar to our previous work [18]. The electron beam is self-focusing due to ion channel effect when it travels in the beam tunnel, which makes the magnetic focusing system unnecessary and minimize the device size [17], [18]. Our group has used the pseudospark plasma cathode in the development of low-cost, compact, and high-power mm-wave and THz VEDs, including a *Ka*-band Cherenkov maser [19], *W*/*G*-band extended interaction oscillators (EIOs) [9], [20], and a *G*-band BWO [18]. We conduct the hot-test analysis of DNPSG BWO

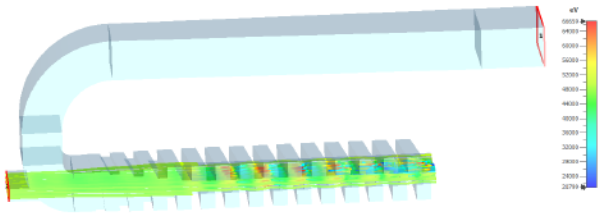

Fig. 6. Sheet beam in the hot-test simulation.

with particle-in-cell (PIC) simulation in CST Particle Studio, and the sheet beam in the interaction space is shown in Fig. 6, in which the beam bunching due to beam–wave interaction is clearly shown by the color variation. The sheet beam will be confined by the ion channel effect in the future experiment, but currently, we use a uniform 2-T longitudinal magnetic field to confine the high-current beam in the simulation due to the difficulty of simultaneous simulation of ion channel focusing in plasma and beam–wave interaction in CST. The beam voltage of 14–90 kV is used in the simulation to analyze the wideband performance, and we adjust the current density in the range of 1.5–5 $\times$ 10^7 A/m^2 (beam current: 12.9–42.9 A) to take into account the current variation over the duration of the beam pulse [18]. A similar variation of the beam voltage and current over time can be found in our previous work [18]. The simulation at constant voltage/current allows knowing the performance at the interaction points, while in the experiment, a swept frequency is expected and the DNPSG BWO will show broadband radiation, considering that the operating beam voltage and current are not constant in the pseudospark discharge. The transverse size of the beam is 2.052 $\times$ 0.418 mm^2, which is the same with the beam tunnel, but the thermal effect of electron collision on the beam tunnel wall is negligible considering that the pseudospark-sourced BWO works in pulsed mode with low repetition rate (a few thousand Hertz) [15], [18].

After the PIC simulation, we obtain the oscillation frequency and output power, as shown in Fig. 7. Fig. 7(a) shows that the oscillation frequency of the DNPSG BWO increases with the operating voltage. The minimum/maximum frequencies are 75 and 113 GHz, at 14 and 90 kV, respectively, i.e., a tuning band of 38 GHz is achieved, covering the entire *W*-band. In contrast, the simulation results of the DSG BWO in Fig. 7(b) show that there is a gap in the frequency band [12] (~50 kV, around 104 GHz) due to mode competition when the electron beam interacts with the high-order mode. To validate this, we present the signals of the DNPSG/DSG BWOs at 50 kV, as shown in Fig. 8. Fig. 8(a) shows that the output signal of the DSG BWO decreases rapidly after 5 ns, while the signal of the DNPSG BWO stays stable. We have also conducted the frequency analysis for the signals in different time spans, as shown in Fig. 8(b). The frequency of the signal from the DNPSG BWO remains stable at 102.2 GHz in 1–5 and 6–10 ns, but the signal frequency of the DSG BWO jumps from 102.7 GHz in 1–5 ns to 146.4 GHz in 6–10 ns with a much smaller peak, showing that the backward oscillation changes from mode 1 to mode 3, according to the illustration of Fig. 2(a) on the interaction between modes in

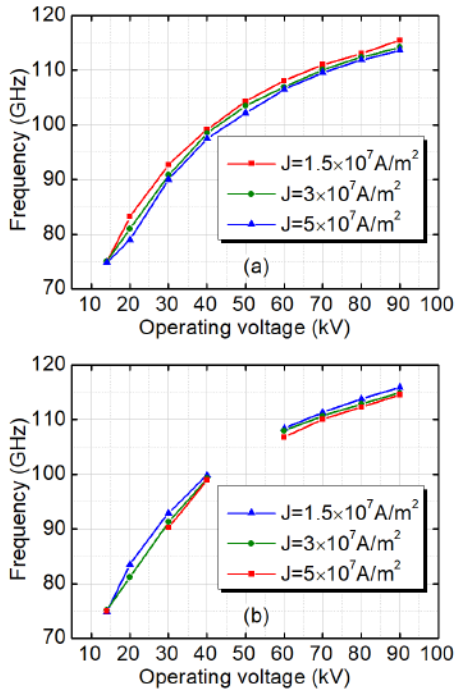

Fig. 7. Simulated oscillation frequency of (a) DNPSG BWO and (b) DSG BWO.

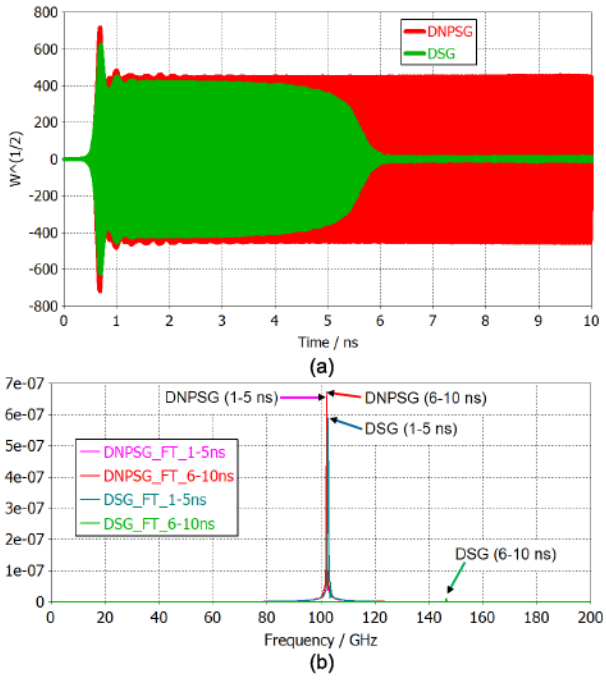

Fig. 8. Signals of DNPSG BWO and DSG BWO at 50 kV and 5 $\times$ 10^7 A/m^2. (a) Time-domain signals and (b) frequency-domain signals for different time spans.

the SWS and the beamlines. So, the bandgap of the DSG BWO is caused by the mode competition, and therefore, tuning band is shortened. The enhanced coupling impedance in the DNPSG SWS is helpful in eliminating the power dip because it enhances the interaction with the lower mode, boosting the power transferred to the desired mode and suppressing the higher modes, which equivalently expands the tuning band. Therefore, the wideband capability of the *W*-band DNPSG BWO is verified.

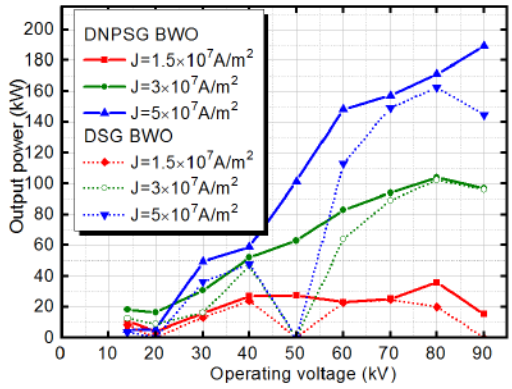

Fig. 9. Simulation results of output power of DNPSG BWO and DSG BWO.

Fig. 9 shows that the output power increases as the current density grows, and the maximum power is 190 kW at 90 kV and 5×10^7 A/m^2 (42.9 A). The power of the DSG BWO is lower than that of the DNPSG BWO, and there is a power dip at ∼50 kV due to mode competition, agreeing with the frequency gap shown in Fig. 7(b) [12]. Therefore, the DNPSG BWO is more robust against mode competition due to its enhanced coupling impedance and could eliminate the potential power dips, thus extending the working frequency band.

Simulation results of the oscillation frequency and power in Figs. 7 and 9 show that high power in a wide band (covering entire *W*-band) in the designed DNPSG BWO is achieved.

IV. Conclusion

This article presents the design of a *W*-band BWO using a novel DNPSG SWS, driven by pseudospark-sourced sheet electron beam. First, the DNPSG SWS is simulated to show a wide BWO band of 72–125 GHz (53 GHz), and its coupling impedance is higher than that in the DSG SWS by 2.3%–55.3%. The complete structure of the BWO is designed and fabricated, consisting of ten DNPSG SWS units and a wideband output structure. The cold test of the DNPSG BWO shows that S_{11} (double of the losses in the DNPSG BWO) is above −10 dB in most of the *W*-band, and its trend agrees with simulation results, which is satisfactory in the pseudospark-driven high-power device.

Then, the hot-test performance of the DNPSG BWO is investigated with PIC simulation in the beam voltage range of 14–90 kV and a beam current density range of $1.5–5 \times 10^7$ A/m^2. An ultrabroad tuning band of 38 GHz (75–113 GHz) and a high output power (max. 190 kW) are obtained, verifying its high power and broadband capability due to enhanced coupling impedance. The hot-test measurement of the *W*-band DNPSG BWO will be conducted in the further study.

References

[1] S. Gilmour, "Introduction," in *Klystrons,Traveling Wave Tubes, Magnetrons, Crossed-Field Amplifiers, and Gyrotrons*. Norwood, MA, USA: Artech House, 2011, pp. 1–2.

[2] J. H. Booske *et al.*, "Vacuum electronic high power terahertz sources," *IEEE Trans. THz Sci. Technol.*, vol. 1, no. 1, pp. 54–75, Sep. 2011, doi: 10.1109/TTHZ.2011.2151610.

[3] L. Zhang, J. Cai, X. Bian, X. Wu, and J. Feng, "A novel THz forward and backward wave two-mode band-edge oscillator," *IEEE Trans. THz Sci. Technol.*, vol. 10, no. 4, pp. 391–396, Jul. 2020, doi: 10.1109/TTHZ.2020.2972291.

[4] Y.-M. Shin, L. R. Barnett, and N. C. Luhmann, "Phase-shifted traveling-wave-tube circuit for ultrawideband high-power submillimeter-wave generation," *IEEE Trans. Electron Devices*, vol. 56, no. 5, pp. 706–712, May 2009, doi: 10.1109/TED.2009.2015404.

[5] C. Paoloni *et al.*, "THz backward-wave oscillators for plasma diagnostic in nuclear fusion," *IEEE Trans. Plasma Sci.*, vol. 44, no. 4, pp. 369–376, Apr. 2016, doi: 10.1109/TPS.2016.2541119.

[6] Q. Liu, Z. Wang, P. Liu, C. Du, H. Li, and A. Xu, "A THz backward-wave oscillator based on a double-grating rectangular waveguide," *IEEE Trans. Electron Devices*, vol. 60, no. 4, pp. 1463–1468, Apr. 2013, doi: 10.1109/TED.2013.2246868.

[7] W. Ge *et al.*, "Transmission characteristics of double staggered grating waveguide SWS: Simulation and measurement," in *Proc. Int. Vac. Electron. Conf. (IVEC)*, Busan, South Korea, Apr. 2019, pp. 1–3, doi: 10.1109/IVEC.2019.8745059.

[8] B. Popovic *et al.*, "346 GHz BWO for fusion plasma diagnostics," in *Proc. 39th Int. Conf. Infr., Millim., THz Waves (IRMMW-THz)*, Sep. 2014, p. 1, doi: 10.1109/IRMMW-THz.2014.6956194.

[9] G. X. Shu *et al.*, "Demonstration of a planar W-band, kW-level extended interaction oscillator based on a pseudospark-sourced sheet electron beam," *IEEE Electron Device Lett.*, vol. 39, no. 3, pp. 432–435, Mar. 2018, doi: 10.1109/LED.2018.2794469.

[10] T. H. Chang, C. F. Yu, C. L. Hung, Y. S. Yeh, M. C. Hsiao, and Y. Y. Shin, "W-band TE_{01} gyrotron backward-wave oscillator with distributed loss," *Phys. Plasmas*, vol. 15, no. 7, Jul. 2008, Art. no. 073105, doi: 10.1063/1.2950305.

[11] J. Xie *et al.*, "Study of a 0.35 THz extended interaction oscillator driven by a pseudospark-sourced sheet electron beam," *IEEE Trans. Electron Devices*, vol. 67, no. 2, pp. 652–658, Feb. 2020, doi: 10.1109/TED.2019.2957760.

[12] J. Zhang, Y. Alfadhl, X. Chen, L. Zhang, and A. W. Cross, "Design of dual-band high-power backward wave oscillator using double staggered grating and pseudospark-sourced sheet beam," in *Proc. 14th U.K.-Europe-China Workshop Millimetre-Waves THz Technol. (UCMMT)*, Sep. 2021, pp. 1–3, doi: 10.1109/UCMMT53364.2021.9569914.

[13] T. A. Karetnikova, A. G. Rozhnev, N. M. Ryskin, A. E. Fedotov, S. V. Mishakin, and N. S. Ginzburg, "Gain analysis of a 0.2-THz traveling-wave tube with sheet electron beam and staggered grating slow wave structure," *IEEE Trans. Electron Devices*, vol. 65, no. 6, pp. 2129–2134, Jun. 2018, doi: 10.1109/TED.2017.2787960.

[14] G. Shu *et al.*, "Dispersion and dielectric attenuation properties of a wideband double-staggered grating waveguide for subterahertz sheet-beam traveling-wave amplifiers," *IEEE Trans. Electron Devices*, vol. 68, no. 11, pp. 5826–5833, Nov. 2021, doi: 10.1109/TED.2021.3110183.

[15] J. Zhang *et al.*, "Study on wideband THz backward wave oscillator driven by pseudospark-sourced sheet electron beam," *IEEE Trans. Electron Devices*, vol. 67, no. 8, pp. 3395–3402, Aug. 2020, doi: 10.1109/TED.2020.3005362.

[16] A. Babaeihaselghobi, M. N. Akram, H. B. Ghavifekr, and L. R. Billa, "A novel chevron-shape double-staggered grating waveguide slow wave structure for terahertz traveling wave tubes," *IEEE Trans. Electron Devices*, vol. 67, no. 9, pp. 3781–3787, Sep. 2020, doi: 10.1109/TED.2020.3006038.

[17] K. Frank and J. Christiansen, "The fundamentals of the pseudospark and its applications," *IEEE Trans. Plasma Sci.*, vol. 17, no. 5, pp. 748–753, Oct. 1989, doi: 10.1109/27.41195.

[18] W. He *et al.*, "Generation of broadband terahertz radiation using a backward wave oscillator and pseudospark-sourced electron beam," *Appl. Phys. Lett.*, vol. 107, no. 13, Sep. 2015, Art. no. 133501, doi: 10.1063/1.4932099.

[19] H. Yin, A. W. Cross, W. He, A. D. R. Phelps, and K. Ronald, "Pseudospark experiments: Cherenkov interaction and electron beam post-acceleration," *IEEE Trans. Plasma Sci.*, vol. 32, no. 1, pp. 233–239, Feb. 2004, doi: 10.1109/TPS.2004.823986.

[20] G. Shu *et al.*, "Experimental demonstration of a terahertz extended interaction oscillator driven by a pseudospark-sourced sheet electron beam," *Appl. Phys. Lett.*, vol. 112, no. 3, Jan. 2018, Art. no. 033504, doi: 10.1063/1.5011102.